Article

Cell Chemical Biology

Deacylation Mechanism by SIRT2 Revealed in the 1′-SH-2′-O-Myristoyl Intermediate Structure

Highlights

- The structure of SIRT2 in complex with a thiomyristoyl lysine peptide inhibitor and NAD is obtained
- The structure captures a new catalytic intermediate (III)
- The new catalytic intermediate provides better understanding of the sirtuin reaction mechanism

Authors

Yi Wang, Yi Man Eva Fung, Weizhe Zhang, ..., Jing Hu, Hening Lin, Quan Hao

Correspondence

hl379@cornell.edu (H.L.), qhao@hku.hk (Q.H.)

In Brief

Sirtuins are NAD-dependent deacylases involved in various important biological pathways. Wang et al. use structural studies to reveal the formation of a new catalytic intermediate, III. Understanding the detailed reaction mechanism may facilitate the development of sirtuin inhibitors as therapeutic reagents or as tool compounds to understand sirtuin biology.

Wang et al., 2017, Cell Chemical Biology *24*, 1–7
March 16, 2017
http://dx.doi.org/10.1016/j.chembiol.2017.02.007

CellPress

Please cite this article in press as: Wang et al., Deacylation Mechanism by SIRT2 Revealed in the 1′-SH-2′-O-Myristoyl Intermediate Structure, Cell Chemical Biology (2017), http://dx.doi.org/10.1016/j.chembiol.2017.02.007

Cell Chemical Biology
Article

Deacylation Mechanism by SIRT2 Revealed in the 1′-SH-2′-O-Myristoyl Intermediate Structure

Yi Wang,[1] Yi Man Eva Fung,[2] Weizhe Zhang,[1,3] Bin He,[4] Matthew Wai Heng Chung,[1] Jing Jin,[1] Jing Hu,[5] Hening Lin,[5,*] and Quan Hao[1,6,*]

[1]School of Biomedical Sciences, University of Hong Kong, Hong Kong, China
[2]State Key Laboratory of Synthetic Chemistry and Department of Chemistry, University of Hong Kong, Hong Kong, China
[3]Shanghai Institutes of Biological Sciences, Chinese Academy of Sciences, Shanghai 200031, China
[4]College of Pharmacy, Engineering Research Center for the Development and Application of Ethnic Medicine and TCM Ministry of Education, Guizhou Medical University, Guizhou 550004, China
[5]Department of Chemistry and Chemical Biology, Howard Hughes Medical Institute, Cornell University, Ithaca, NY 14853, USA
[6]Lead Contact
*Correspondence: hl379@cornell.edu (H.L.), qhao@hku.hk (Q.H.)
http://dx.doi.org/10.1016/j.chembiol.2017.02.007

SUMMARY

Sirtuins are NAD-dependent deacylases. Previous studies have established two important enzymatic intermediates in sirtuin-catalyzed deacylation, an alkylamidate intermediate I, which is then converted to a bicyclic intermediate II. However, how intermediate II is converted to products is unknown. Based on potent SIRT2-specific inhibitors we developed, here we report crystal structures of SIRT2 in complexes with a thiomyristoyl lysine peptide-based inhibitor and carba-NAD or NAD. Interestingly, by soaking crystals with NAD, we capture a distinct covalent catalytic intermediate (III) that is different from the previously established intermediates I and II. In this intermediate, the covalent bond between the S and the myristoyl carbonyl carbon is broken, and we believe this intermediate III to be the decomposition product of II en route to form the end products. MALDI-TOF data further support the intermediate III formation. This is the first time such an intermediate has been captured by X-ray crystallography and provides more mechanistic insights into sirtuin-catalyzed reactions.

INTRODUCTION

Mammalian sirtuins (SIRT1–7) are nicotinamide adenine dinucleotide (NAD)-dependent enzymes that catalyze the removal of acyl groups from lysine residues on substrates (Bouras et al., 2005; Daitoku et al., 2004; Motta et al., 2004; Starai et al., 2002). They were established initially as deacetylase on histones, transcription factors, and metabolic enzymes (Imai et al., 2000; Katto et al., 2013; Tao et al., 2013). However, recently they have been shown to be able to remove a variety of different acyl lysine modifications. SIRT1–3 are able to depropionylate and debutyrylate lysines (Garrity et al., 2007; Smith and Denu, 2007). SIRT3 was also reported to have decrotonylation activity. SIRT4 was recently shown as a lipoamidase regulating pyruvate dehydrogenase complex activity, despite the enzymatic activity being very inefficient in vitro (Bao et al., 2014; Mathias et al., 2014). SIRT5 was reported to hydrolyze succinyl, malonyl, and glutaryl lysines (Du et al., 2011; Roessler et al., 2014; Tan et al., 2014). SIRT6 can efficiently remove long-chain fatty acyl groups on tumor necrosis factor α (Jiang et al., 2013). Interestingly, recent studies also demonstrated that SIRT2 is a defatty-acylase (Feldman et al., 2013; Jin et al., 2016; Liu et al., 2015; Teng et al., 2015). These findings have broadened the substrate scope of sirtuins and provided important insights into the diverse biological functions of sirtuins and novel protein lysine acylations.

All sirtuins share a conserved core region, composed of one NAD-binding Rossmann domain and a zinc-binding domain, suggesting a similar catalytic mechanism for all sirtuins. The catalytic mechanism of sirtuin-catalyzed deacylation (Figure 1) has been well established (Sauve et al., 2001; Sauve and Youn, 2012). The first step of the reaction is the formation of an alkylamidate intermediate (I) between NAD and the acyl lysine substrate, with the release of nicotinamide. A key conserved catalytic His residue then deprotonates the 2′-OH of the ribose, which then attacks the amidate carbon to form a bicyclic intermediate (II). The bicyclic intermediate then decomposes to generate the products, the deacylated lysine and 2′-O-acyl ADPR. Structural studies later provided excellent support for this mechanism. For example, the Michaelis complex that contained both substrates, the acyl lysine peptide and NAD, showed that the amide bond of the acyl lysine substrate is correctly positioned to react with the 1′ position of the ribose of NAD, while the catalytic histidine residue is positioned to deprotonate the 2′- or 3′-OH (Hoff et al., 2006). Furthermore, using mechanism-based sirtuin inhibitors, thioacetyl-lysine peptides, researchers were able to capture the two proposed intermediates, I and II (Figure 1) (Hawse et al., 2008; He et al., 2012; Jin et al., 2009; Zhou et al., 2012).

From intermediate II to the products, it is generally thought that water directly attacks intermediate II, leading to the release of the deacylated peptide. However, no direct experimental evidence exists to support this. Additionally a dioxonium ion intermediate was proposed based on studies for organic reactions, but there has been no direct experimental evidence for the dioxomium ion

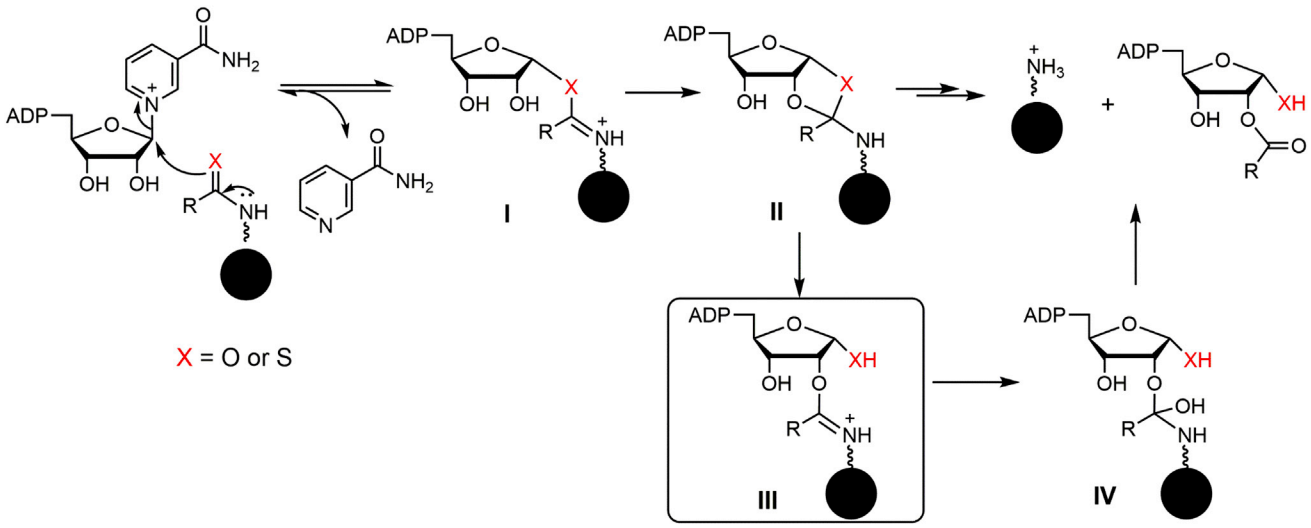

Figure 1. The Catalytic Mechanism for Sirtuin-Catalyzed Deacylation Reactions

in the enzymatic reactions of sirtuins (Sauve and Youn, 2012). Here we report a crystal structure of SIRT2 crystallized with a thiomyristoyl lysine peptide-based inhibitor and NAD. This structure captured a novel intermediate (III, Figure 1) that provides insights into how intermediate II decomposes to form the end products.

RESULTS

We previously developed a potent SIRT2 inhibitor and also obtained a structure of SIRT2 in complex with it (PKK(TMy)TG), referred to as BHJH-TM1 by Teng and colleagues (Jing et al., 2016; Teng et al., 2015). To obtain more information about the catalytic mechanism, we soaked the SIRT2/BHJH-TM1 crystals with carba-NAD or NAD to get potential catalytic intermediates (Table 1). We also co-crystallized SIRT2 with native (i.e., non-thio-modified) myristoyl peptides, but could not obtain any crystals. Denu and co-workers had also tried this experiment but the products, instead of intermediates, were observed inside the catalytic pocket (Feldman et al., 2015). It is very likely that the complex of SIRT2 with the native myristoyl peptide is unstable.

The Crystal Structure of SIRT2 in Complex with BHJH-TM1 and Carba-NAD

Carba-NAD is a non-cleavable analog of NAD and thus may facilitate the capture of a Michaelis complex (Hoff et al., 2006; Szczepankiewicz et al., 2012). The crystal structure of SIRT2 in complexes with the TM peptide BHJH-TM1 and carba-NAD was determined at 1.8-Å resolution (Figures 2A and S1). The electron density for carba-NAD and BHJH-TM1 is well defined (Figure 2B). The overall binding of acyl peptide and carba-NAD superimposed well with that in other ternary sirtuin complexes (Figure S1) (Sanders et al., 2007; Szczepankiewicz et al., 2012). The carba-NAD is in an unproductive conformation, as the distance between the S atom and 1′-C from the N-ribose is not close enough to allow the subsequent nucleophilic attack at the 1′ position (Figure 2C). Meanwhile, the 3′-OH group of the ribose forms moderate hydrogen bonds with the S atom of BHJH-TM1 and NH from the catalytic His, while the distance between 2′-OH and the S atom is relatively far away.

The Crystal Structure of SIRT2 in Complex with BHJH-TM1 and NAD

To capture potential reaction intermediates, we soaked the crystals of SIRT2 in complex with BHJH-TM1 in 10 mM NAD overnight. The resulting crystal diffracted to 1.5-Å resolution, which allowed us to confidently solve the structure. Surprisingly, a novel intermediate (III) was captured that is different from the intermediates I and II that were trapped in SIRT3 and SIRT5 structures, respectively. A $2F_o$-F_c omit map clearly defined the covalent linkage between ADP-ribose and BHJH-TM1. The 2′-O from the N-ribose is covalently bonded to the carbonyl carbon of myristoyl with a bond length of 1.4 Å. The ADP-ribose in intermediate III superimposed well with the ADP-ribose in the SIRT5 bicyclic intermediate II (Figures 3A and 3B). The zoom-in comparison shows that the covalent bond between the S atom and the myristoyl carbonyl carbon is broken (Figure 3B). The distance between these two atoms is 3.3 Å in contrast to the 1.8-Å distance in the SIRT5 bicyclic intermediate II (Figure 3B). Meanwhile, the structure convincingly shows the electron density for the 1′-SH, which is no longer connected to the myristoyl group (Figures 3C and 3D). Thus, the X-ray structural data suggest that the intermediate III we captured is 1′-SH-2′-O-myristoyl ADPR (Figure 1). The formation of intermediate III indicates that intermediate II has undergone another step toward the formation of end products (Figure 1). The bicyclic intermediate II is an intermediate that interconverts I and III. A water molecule can react with III in a way similar to the 2′-OH reacting with I, forming a tetrahedral intermediate (IV), which then can decompose to form the end products.

The Formation of Intermediate III Analyzed by MALDI-TOF Mass Spectrometry

We then used MALDI-TOF mass spectrometry (MS) to analyze the covalent intermediate III directly from the crystals of SIRT2

Table 1. Crystallographic Data and Model Refinement Parameters

	SIRT2/BHJH-TM1/Carba-NAD (PDB: 4X3P)	SIRT2/BHJH-TM1/NAD (PDB: 4X3O)
Wavelength (Å)	0.9793	0.9791
Resolution range (Å)	50–1.8 (1.864–1.799)	50–1.5 (1.553–1.499)
Space group	P 1 2_1 1	P 1 2_1 1
Unit cell	a = 37.6, b = 77.7, c = 56.5 Å, $\alpha = 90°$, $\beta = 97.73°$, $\gamma = 90°$	a = 37.4, b = 77.6, c = 56.2 Å, $\alpha = 90°$, $\beta = 97.22°$, $\gamma = 90°$
Total reflections	366,081	345,257
Unique reflections	29,603 (2,868)	49,246 (3,898)
Multiplicity	3.7	4.1
Completeness (%)	99 (99)	99 (99)
Mean I/σ(I)	19.29 (5.13)	16.72 (2.86)
R_{merge}	0.073	0.069
R_{work}	0.1540 (0.1357)	0.1211 (0.1530)
R_{free}	0.1732 (0.1499)	0.1566 (0.2052)
Protein residues	302	303
RMSD (bonds Å)	0.014	0.01
RMSD (angles °)	1.45	1.53
Ramachandran favored (%)	98	98
Average B factor	25.8	19.8
Macromolecules	25.1	18.1
Ligands	20.9	17.4
Solvent	33.5	35.4

Highest-resolution shell is shown in parentheses. RMSD, root-mean-square deviation.

in complex with TM peptide BHJH-TM1 soaked with NAD. Indeed, ions with *m/z* of 1,296.65, which corresponded to the mass of the protonated species of intermediate III, were detected (Figures 3E and 3G). Additionally we found the ions with *m/z* of 530.33, which corresponded to the mass of the protonated end product, indicating that this intermediate is able to form the end product (Figures 3F and 3G) and is not an off-pathway process. These MS data further support the formation of this intermediate during the SIRT2 catalytic process.

The alkylamidate intermediate III is more stable than the previously proposed dioxonium ion intermediate because the cation can be delocalized by two O and one N atoms, while in the dioxonium the cation can only be delocalized by two O atoms. Thus, it is more likely to form in sirtuin-catalyzed reactions. Furthermore, intermediate III is similar to intermediate I in the sense that both are alkylamidate (or S-alkylamidate), with the only difference being that I involves the 1′ position of the N-ribose while III involves the 2′ position of the N-ribose. The reason we could trap the new intermediate is similar to why the previous intermediates were trapped. The substitution of O with S makes the intermediates more stable (Hawse et al., 2008).

DISCUSSION

Our X-ray structural studies revealed the formation of a new catalytic intermediate, III, which was not previously proposed in sirtuin mechanistic studies (Figure 1). This represents a downstream intermediate and is one step closer to the formation of the end products compared with intermediate II. It explained how intermediate II is converted to products. Thus, we can now further refine the catalytic mechanism of sirtuin-catalyzed deacylation reactions (Figure 1). Structural studies using mechanism-based inhibitors (thioacetyl-lysine peptides) have now provided experimental support for almost all of the reaction intermediates (Figure 4). The current structure of SIRT2 crystallized with TM peptide/carba-NAD showed the initial catalytic step (Figure 4A). The structure of Sir2Tm thioacetyl peptides captured intermediate I (green in Figure 4B). Gertz et al. (2013) reported another structure showing the intermediate I obtained by soaking SIRT3/acetyl-peptide crystals with NAD and inhibitor Ex-243. In this intermediate, however, the ribose is flipped (blue in Figure 4B). The structure of SIRT5 crystallized with a thiosuccinyl peptide captured intermediate II (Figure 4C), while the current SIRT2 structure crystallized with a TM peptide and NAD captured intermediate III (Figure 4D). Given that sirtuins are involved in various important biological pathways, understanding their detailed reaction mechanism may facilitate the development of sirtuin inhibitors as therapeutic reagents or as tool compounds to understand sirtuin biology.

SIGNIFICANCE

The coupling of nicotinamide adenine dinucleotide (NAD^+) breakdown and protein deacylation is a unique feature of the family of proteins named Sirtuins, which are a class of "eraser" enzymes. They regulate energy metabolism, aging and longevity in diverse organisms and are also considered as promising targets for treating several human diseases. There are seven human sirtuins (SIRT1–7). Understanding the catalytic mechanism of sirtuins may facilitate the design

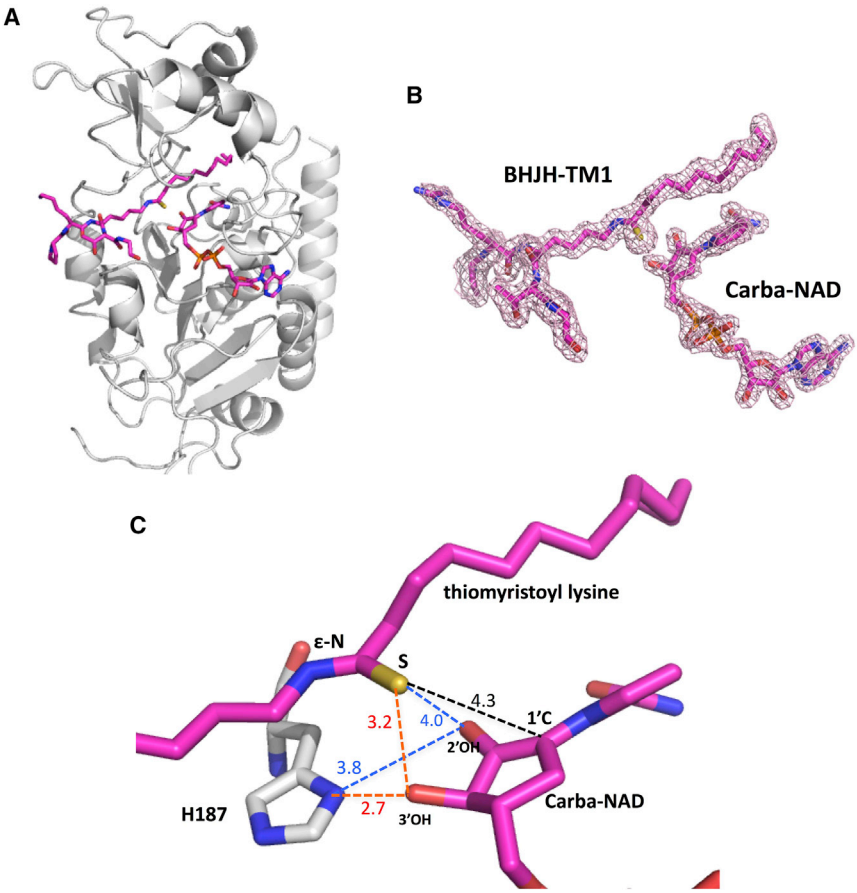

Figure 2. The Structure of SIRT2 with BHJH-TM1 and Carba-NAD

(A) Overall structure.

(B) $2F_o$-F_c omit map (1σ) showing the BHJH-TM1 and carba-NAD.

(C) The relative positions of the BHJH-TM1, carba-NAD, and catalytic His of SIRT2. The unit of bond length is angstroms.

of modulators to treat relevant diseases. In this study, we have captured a novel catalytic intermediate of SIRT2 by X-ray crystallography and confirmed it by MALDI-TOF mass spectrometry. This is the first time such an intermediate has been captured by X-ray crystallography. Previous studies have established two sirtuin enzymatic intermediates, an alkylamidate intermediate I, which is then converted to a bicyclic intermediate II en route to form the final products. However, how intermediate II is converted to products is not known. The new intermediate, III, was captured by soaking the crystal of SIRT2 and a thiomyristoyl inhibitor (BHJH-TM) complex with NAD. This intermediate III represents the decomposition product of II en route to form the final reaction products. This discovery provides significant mechanistic insights into the enzymatic reaction mechanism of sirtuins.

EXPERIMENTAL PROCEDURES

Reagents and Material

Unless otherwise noted, all the chemical reagents were purchased from Sigma-Aldrich. DMEM was purchased from Invitrogen. EDTA-free protease inhibitor was purchased from Roche Applied Science. Pre-stained protein ladder was purchased from Thermo Fisher Scientific. Liquid chromatography-mass spectrometry (LC-MS) was carried out on a Shimadzu LC and Thermo LCQ Fleet MS with a Sprite TARGA C18 column (40 × 2.1 mm, 5 μm, Higgins Analytical) monitoring at 215 and 260 nm. Solvents used in LC-MS were water with 0.1% acetic acid and acetonitrile with 0.1% acetic acid. Analytical high-performance liquid chromatography (HPLC) analysis was carried out using a Kinetex XB-C18 100A, 100 × 4.60-mm, 2.6-μm reverse-phase column with UV detection at 215 and 280 nm. Preparative HPLC purification was carried out using Targa Prep C18 250 × 20-mm, 10-μm reverse-phase column with UV detection at 215 and 260 nm.

Solid Synthesis of Peptides

Synthesis of peptides of BHJH-TM1 was carried out using the protocol of Jing et al. (2016). Thiomyristoyl peptide was synthesized using the standard Fmoc/tBu chemistry O-benzotriazol-N,N,N′,N′-tetramethyluronium hexafluorophosphate/1-hydroxybenzotriazol (HBTU/HOBt) protocol with Wang resin. Modified lysine was incorporated using L-Fmoc-Lys(thiomyristoyl)-OH. Cleavage from the resin and removal of all protecting groups were done by incubating the resin with trifluoroacetic acid (TFA) containing phenol (5%), thioanisole (5%), ethanedithiol (2.5%), and water (5%) for 2 hr. The crude peptide was purified by reverse-phase HPLC on a Beckman Coulter System Gold 125P solvent module and 168 Detector with a Targa C18 column (250 × 20 mm, 10 μm, Higgins Analytical) monitoring at 215 nm. Mobile phases used were 0.1% aqueous TFA (solvent A) and 0.1% TFA in acetonitrile (solvent B). Flow rate was 10 mL/min by using the following gradient: 0% solvent B for 10 min, 0%–50% solvent B over 50 min, then 50%–95% solvent B for 5 min. The identity and purity of the peptides were verified by LC-MS. BHJH-TM1 (PKK(TMy)TG) was eluted at 55 min. LC-MS (electrospray ionization) calcd. for $C_{37}H_{70}N_7O_7S$ $[M + H]^+$ 756.51, obsd. 756.58.

Expression and Purification of Truncated SIRT2 for Crystallization

SIRT2 expression and purification was carried out as per reported protocol (Teng et al., 2015). The open reading frame of human SIRT2 (34–356) was inserted into a pET28a-sumo vector between the BamHI and NotI sites. SIRT2 was overexpressed in *Escherichia coli* BL21 (DE3) grown in LB culture medium. Isopropyl β-D-1-thiogalactopyranoside (0.2 mM) was used to induce expression when the OD value was 0.6. Bacteria were collected after growth for another 20 hr at 289 K. After sonication, the supernatant was loaded onto a nickel column pre-equilibrated with 20 mM HEPES (pH 7.0) with 500 mM NaCl. The protein was eluted with a linear gradient of imidazole. The eluted protein fractions were cleaved by ULP1 overnight and then loaded onto an Ni-nitrilotriacetic acid column. The collected protein fraction in flow-through was concentrated and loaded onto Superdex200 to obtain further purification. The peak containing SIRT2 was pooled, concentrated to 8 mg/mL, and stored at −80°C.

Crystallization, Data Collection, and Structural Determination

Crystals of SIRT2 in complex with 1 mM TM peptide (PKK(Tmy)TG), BHJH-TM1, were obtained by hanging-drop vapor diffusion method at 291 K. A solution containing 8 mg/mL SIRT2 in 20 mM HEPES (pH 7.0) and 100 mM NaCl was pre-incubated on ice with 1 mM BHJH-TM1 for about 1 hr. Hanging drops were formed by mixing 1 μL of protein solution and 1 μL of well solution containing 1.6 M $(NH_4)_2SO_4$, 0.1 M HEPES buffer (pH 7.0), and 5% glycerol. Crystals were soaked with 10 mM carba-NAD and NAD,

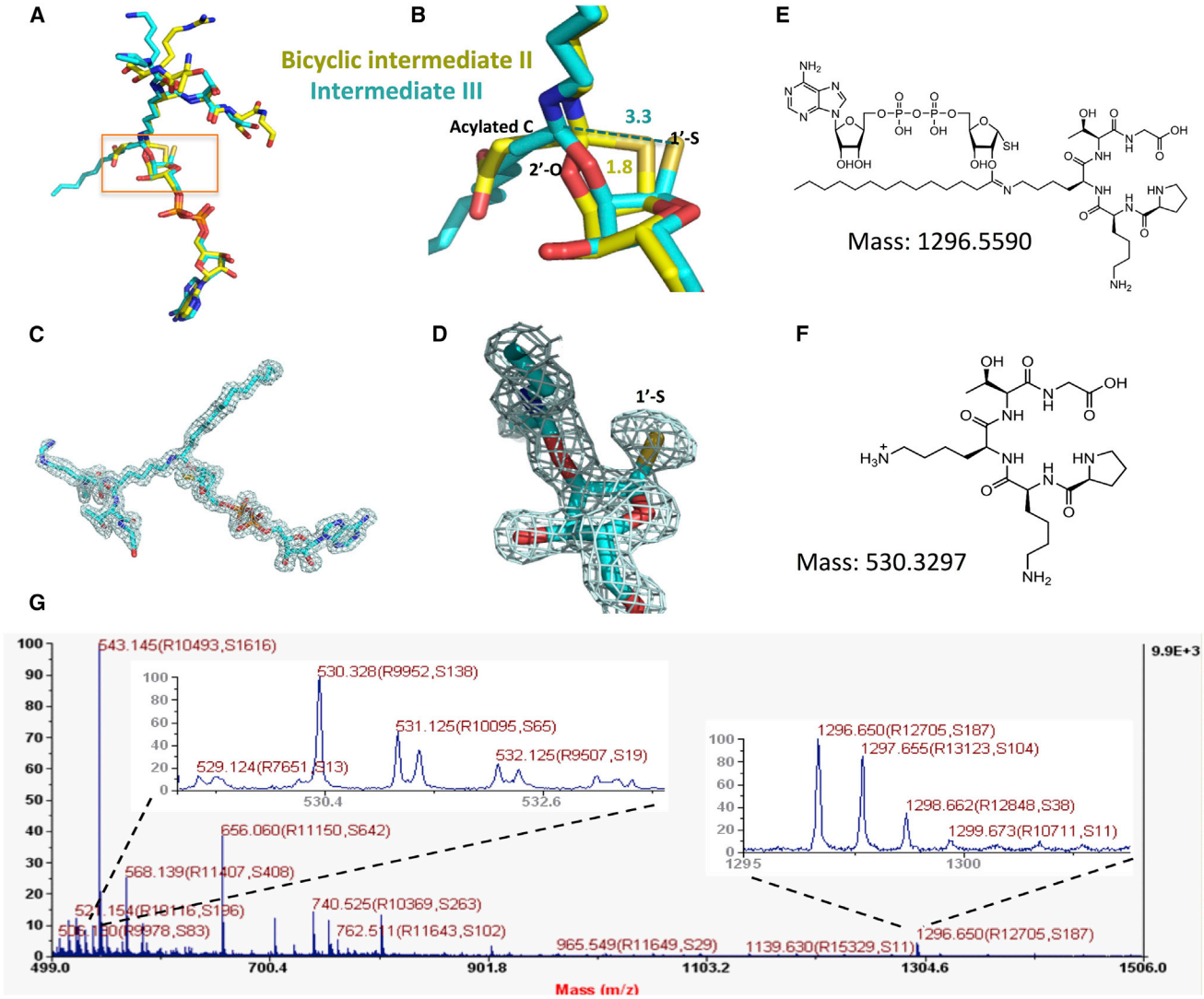

Figure 3. The Intermediate III in SIRT2/BHJH-TM1/NAD Complex Structure

(A and B) Comparison between SIRT5 intermediate II structure (yellow) and SIRT2 intermediate III structure (cyan). The unit of bond length is angstroms.

(C and D) $2F_o$-F_c omit map (1σ) showing the linkage between the BHJH-TM1 and ADP-ribose.

(E and F) The chemical formulas and molecular weights of intermediate III from the reaction of BHJH-TM1 with NAD and the end product.

(G) MALDI-TOF MS spectrum of the crystals of SIRT2 in complex with thiomyristoyl peptide BHJH-TM1 soaked with NAD, using α-cyano-4-hydroxycinnamic acid as matrix. The mass ranges corresponding to both intermediate III and the end product are enlarged.

respectively for 1–8 hr. After data collection at the synchrotron, data were indexed and integrated by using the HKL2000 program (Otwinowski and Minor, 1997). The complex structure was solved by molecular replacement using the program Phaser (McCoy et al., 2007) from the CCP4 suite (Bailey et al., 1994) with the SIRT2 binary structure (PDB: 4R8M) as the search model. Refinement and ligand fitting were performed with REFMAC and Coot from CCP4. Data collection and structure refinement statistics are shown in Table 1. Atomic coordinates and structure factors have been deposited with the PDB under accession codes PDB: 4X3P (SIRT2 in complexes with BHJH-TM1 and carba-NAD) and PDB: 4X3O (SIRT2 with intermediate III).

MALDI-TOF MS Analysis

The positive Reflector mode of the MALDI-TOF MS instrument was used. Crystals of SIRT2 in complex with TM peptide BHJH-TM1 soaked with NAD overnight was mixed with α-cyano-4-hydroxycinnamic acid (CHCA) and deposited onto a MALDI sample plate. The samples were spotted and dried on the MALDI plate before applying 1 μL of 10 mg/mL CHCA matrix (Fluka; catalog #28480) dissolved in 0.1% formic acid/50% acetonitrile. Mass determination was performed using the 4800 MALDI-TOF/TOF Analyzer (Sciex), which was equipped with an Nd:YAG laser operating at 355 nm to ionize the samples. All mass spectra were acquired in positive ion Reflector mode using the 4000 Series Explorer version 3.5.28193 software (Sciex). Before each run, the mass spectrum was calibrated using the peptide calibration standard, 4700 Cal-Mix (Sciex; catalog #4333604). Characteristic spectra were attained by averaging 500 acquisitions in Reflector mode with the smallest amount possible of laser energy to maintain the best resolution. The scanning range was from *m/z* 500 to 1,500.

SUPPLEMENTAL INFORMATION

Supplemental Information includes one figure and can be found with this article online at http://dx.doi.org/10.1016/j.chembiol.2017.02.007.

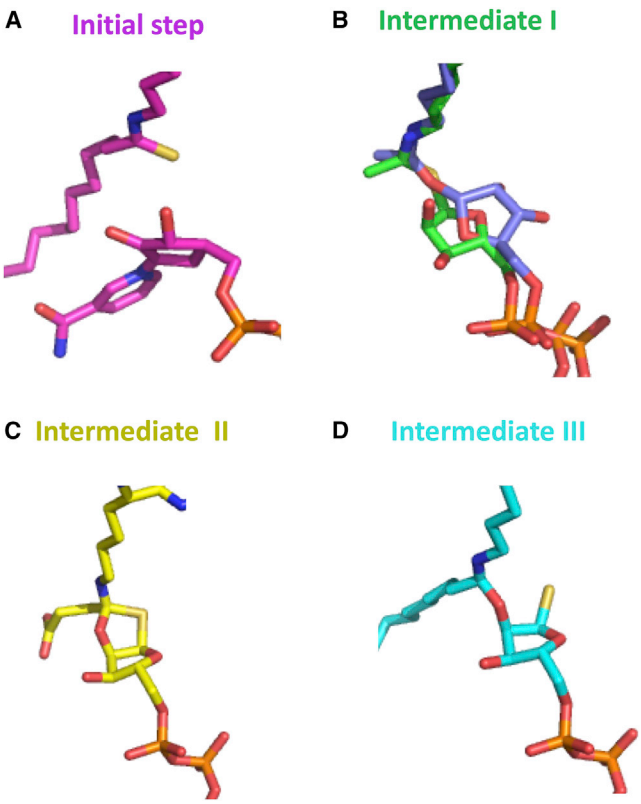

Figure 4. The Catalytic Mechanism Shown by Specific Intermediate Structures

(A) PDB: 4X3P (magenta, SIRT2) for initial step.
(B) PDB: 3D81 (green, Sir2Tm) and PDB: 4BVG (blue, SIRT3) for intermediate I.
(C) PDB: 4F56 (yellow, SIRT5) for intermediate II.
(D) PDB: 4X3O (cyan, SIRT2) for intermediate III.

AUTHOR CONTRIBUTIONS

Y.W., H.L., and Q.H. conceived the idea and Y.W. conducted the structural experiments. Y.M.E.F. analyzed the mass data. W.Z. refined structures and deposited the data. B.H. and J.H. synthesized peptides. Y.W., Y.M.E.F., J.J., M.W.H.C., B.H., H.L., and Q.H. wrote and reviewed the manuscript. Q.H. coordinated the collaboration.

ACKNOWLEDGMENTS

This work was supported in part by HK-RGC C7037-14G (Q.H.) and NIH R01 GM098596 (H.L.). The crystallographic data were collected on BL17U of the Shanghai Synchrotron Radiation Facility. The MALDI-TOF data were collected at the HKU Center for Genomic Sciences.

Received: November 3, 2016
Revised: January 4, 2017
Accepted: February 1, 2017
Published: March 9, 2017

REFERENCES

Bailey, S., Fairlamb, A.H., and Hunter, W.N. (1994). Structure of trypanothione reductase from *Crithidia fasciculata* at 2.6 A resolution; enzyme-NADP interactions at 2.8 A resolution. Acta Crystallogr. D Biol. Crystallogr. *50*, 139–154.

Bao, X., Wang, Y., Li, X., Li, X.M., Liu, Z., Yang, T., Wong, C.F., Zhang, J., Hao, Q., and Li, X.D. (2014). Identification of 'erasers' for lysine crotonylated histone marks using a chemical proteomics approach. ELife *3*, e02999.

Bouras, T., Fu, M., Sauve, A.A., Wang, F., Quong, A.A., Perkins, N.D., Hay, R.T., Gu, W., and Pestell, R.G. (2005). SIRT1 deacetylation and repression of p300 involves lysine residues 1020/1024 within the cell cycle regulatory domain 1. J. Biol. Chem. *280*, 10264–10276.

Daitoku, H., Hatta, M., Matsuzaki, H., Aratani, S., Ohshima, T., Miyagishi, M., Nakajima, T., and Fukamizu, A. (2004). Silent information regulator 2 potentiates Foxo1-mediated transcription through its deacetylase activity. Proc. Natl. Acad. Sci. USA *101*, 10042–10047.

Du, J., Zhou, Y., Su, X., Yu, J.J., Khan, S., Jiang, H., Kim, J., Woo, J., Kim, J.H., Choi, B.H., et al. (2011). Sirt5 is a NAD-dependent protein lysine demalonylase and desuccinylase. Science *334*, 806–809.

Feldman, J.L., Baeza, J., and Denu, J.M. (2013). Activation of the protein deacetylase SIRT6 by long-chain fatty acids and widespread deacylation by mammalian sirtuins. J. Biol. Chem. *288*, 31350–31356.

Feldman, J.L., Dittenhafer-Reed, K.E., Kudo, N., Thelen, J.N., Ito, A., Yoshida, M., and Denu, J.M. (2015). Kinetic and structural basis for acyl-group selectivity and NAD(+) dependence in sirtuin-catalyzed deacylation. Biochemistry *54*, 3037–3050.

Garrity, J., Gardner, J.G., Hawse, W., Wolberger, C., and Escalante-Semerena, J.C. (2007). N-lysine propionylation controls the activity of propionyl-CoA synthetase. J. Biol. Chem. *282*, 30239–30245.

Gertz, M., Fischer, F., Nguyen, G.T., Lakshminarasimhan, M., Schutkowski, M., Weyand, M., and Steegborn, C. (2013). Ex-527 inhibits Sirtuins by exploiting their unique NAD+-dependent deacetylation mechanism. Proc. Natl. Acad. Sci. USA *110*, E2772–E2781.

Hawse, W.F., Hoff, K.G., Fatkins, D.G., Daines, A., Zubkova, O.V., Schramm, V.L., Zheng, W., and Wolberger, C. (2008). Structural insights into intermediate steps in the Sir2 deacetylation reaction. Structure *16*, 1368–1377.

He, B., Du, J., and Lin, H. (2012). Thiosuccinyl peptides as Sirt5-specific inhibitors. J. Am. Chem. Soc. *134*, 1922–1925.

Hoff, K.G., Avalos, J.L., Sens, K., and Wolberger, C. (2006). Insights into the sirtuin mechanism from ternary complexes containing NAD^+ and acetylated peptide. Structure *14*, 1231–1240.

Imai, S., Armstrong, C.M., Kaeberlein, M., and Guarente, L. (2000). Transcriptional silencing and longevity protein Sir2 is an NAD-dependent histone deacetylase. Nature *403*, 795–800.

Jiang, H., Khan, S., Wang, Y., Charron, G., He, B., Sebastian, C., Du, J., Kim, R., Ge, E., Mostoslavsky, R., et al. (2013). SIRT6 regulates TNF-alpha secretion through hydrolysis of long-chain fatty acyl lysine. Nature *496*, 110–113.

Jin, L., Wei, W., Jiang, Y., Peng, H., Cai, J., Mao, C., Dai, H., Choy, W., Bemis, J.E., Jirousek, M.R., et al. (2009). Crystal structures of human SIRT3 displaying substrate-induced conformational changes. J. Biol. Chem. *284*, 24394–24405.

Jin, J., He, B., Zhang, X., Lin, H., and Wang, Y. (2016). SIRT2 reverses 4-oxononanoyl lysine modification on histones. J. Am. Chem. Soc. *138*, 12304–12307.

Jing, H., Hu, J., He, B., Negron Abril, Y.L., Stupinski, J., Weiser, K., Carbonaro, M., Chiang, Y.L., Southard, T., Giannakakou, P., et al. (2016). A SIRT2-selective inhibitor promotes c-Myc oncoprotein degradation and exhibits broad anticancer activity. Cancer Cell *29*, 767–768.

Katto, J., Engel, N., Abbas, W., Herbein, G., and Mahlknecht, U. (2013). Transcription factor NFkappaB regulates the expression of the histone deacetylase SIRT1. Clin. Epigenetics *5*, 11.

Liu, Z., Yang, T., Li, X., Peng, T., Hang, H.C., and Li, X.D. (2015). Integrative chemical biology approaches for identification and characterization of "erasers" for fatty-acid-acylated lysine residues within proteins. Angew. Chem. Int. Ed. Engl. *54*, 1149–1152.

Mathias, R.A., Greco, T.M., Oberstein, A., Budayeva, H.G., Chakrabarti, R., Rowland, E.A., Kang, Y., Shenk, T., and Cristea, I.M. (2014). Sirtuin 4 is a lipoamidase regulating pyruvate dehydrogenase complex activity. Cell *159*, 1615–1625.

McCoy, A.J., Grosse-Kunstleve, R.W., Adams, P.D., Winn, M.D., Storoni, L.C., and Read, R.J. (2007). Phaser crystallographic software. J. Appl. Crystallogr. *40*, 658–674.

Motta, M.C., Divecha, N., Lemieux, M., Kamel, C., Chen, D., Gu, W., Bultsma, Y., McBurney, M., and Guarente, L. (2004). Mammalian SIRT1 represses forkhead transcription factors. Cell *116*, 551–563.

Otwinowski, Z., and Minor, W. (1997). [20] Processing of X-ray diffraction data collected in oscillation mode. Methods Enzymol. *276*, 307–326.

Roessler, C., Nowak, T., Pannek, M., Gertz, M., Nguyen, G.T., Scharfe, M., Born, I., Sippl, W., Steegborn, C., and Schutkowski, M. (2014). Chemical probing of the human sirtuin 5 active site reveals its substrate acyl specificity and peptide-based inhibitors. Angew. Chem. Int. Ed. Engl. *53*, 10728–10732.

Sanders, B.D., Zhao, K., Slama, J.T., and Marmorstein, R. (2007). Structural basis for nicotinamide inhibition and base exchange in Sir2 enzymes. Mol. Cell *25*, 463–472.

Sauve, A.A., and Youn, D.Y. (2012). Sirtuins: NAD(+)-dependent deacetylase mechanism and regulation. Curr. Opin. Chem. Biol. *16*, 535–543.

Sauve, A.A., Celic, I., Avalos, J., Deng, H., Boeke, J.D., and Schramm, V.L. (2001). Chemistry of gene silencing: the mechanism of NAD^+-dependent deacetylation reactions. Biochemistry *40*, 15456–15463.

Smith, B.C., and Denu, J.M. (2007). Acetyl-lysine analog peptides as mechanistic probes of protein deacetylases. J. Biol. Chem. *282*, 37256–37265.

Starai, V.J., Celic, I., Cole, R.N., Boeke, J.D., and Escalante-Semerena, J.C. (2002). Sir2-dependent activation of acetyl-CoA synthetase by deacetylation of active lysine. Science *298*, 2390–2392.

Szczepankiewicz, B.G., Dai, H., Koppetsch, K.J., Qian, D., Jiang, F., Mao, C., and Perni, R.B. (2012). Synthesis of carba-NAD and the structures of its ternary complexes with SIRT3 and SIRT5. J. Org. Chem. *77*, 7319–7329.

Tan, M., Peng, C., Anderson, K.A., Chhoy, P., Xie, Z., Dai, L., Park, J., Chen, Y., Huang, H., Zhang, Y., et al. (2014). Lysine glutarylation is a protein posttranslational modification regulated by SIRT5. Cell Metab. *19*, 605–617.

Tao, R., Xiong, X., DePinho, R.A., Deng, C.X., and Dong, X.C. (2013). FoxO3 transcription factor and Sirt6 deacetylase regulate low density lipoprotein (LDL)-cholesterol homeostasis via control of the proprotein convertase subtilisin/kexin type 9 (Pcsk9) gene expression. J. Biol. Chem. *288*, 29252–29259.

Teng, Y.B., Jing, H., Aramsangtienchai, P., He, B., Khan, S., Hu, J., Lin, H., and Hao, Q. (2015). Efficient demyristoylase activity of SIRT2 revealed by kinetic and structural studies. Sci. Rep. *5*, 8529.

Zhou, Y., Zhang, H., He, B., Du, J., Lin, H., Cerione, R.A., and Hao, Q. (2012). The bicyclic intermediate structure provides insights into the desuccinylation mechanism of human sirtuin 5 (SIRT5). J. Biol. Chem. *287*, 28307–28314.